21

Features of terahertz radiation generation and interaction with sodium acid phthalate (NaAP) crystal

© F.A. Kozhevnikov[1], V.L. Manomenova[2], E.B. Rudneva[2], N.N. Kozlova[2], A.S. Sinko[1,2]

[1] Moscow State University, Moscow, Russia
[2] National Research Center „Kurchatov Institute“, Moscow, Russia

Received June 02, 2025
Revised August 27, 2025
Accepted September 19, 2025

A novel terahertz molecular crystal, sodium acid phthalate (NaAP), has been investigated. The high-Q infrared (IR) and Raman-active vibrational modes of NaAP crystal in the terahertz frequency range enable the generation of narrowband terahertz radiation when the medium is excited by ultrashort laser pulses. It has been established that the spectral characteristics of absorption and refraction in the terahertz range strongly depend on temperature and crystal orientation. The obtained results suggest that NaAP crystal is a promising nonlinear optical material for terahertz photonics and optoelectronics.

Keywords: terahertz radiation, molecular crystal, terahertz spectroscopy, nonlinear optical generation.

DOI: 10.61011/EOS.2025.09.62313.8346-25

Introduction

The terahertz frequency range (0.1−10 THz) attracts significant scientific and technological interest due to its unique application possibilities. These include fundamental studies of new magnetoactive, dielectric, and biological materials [1], as well as practical tasks such as space monitoring systems [2], substance identification by their characteristic spectral „fingerprint“ [3], nondestructive testing, and security systems [4]. In recent years, alongside broadband systems, there has been growing demand for efficient and compact narrowband terahertz sources. These are essential for the development of highly selective resonant spectroscopy, nonlinear terahertz photonics, and advanced high-speed wireless communication systems.

One approach to creating terahertz sources is based on nonlinear optical effects in crystals. Various materials are studied for this purpose: inorganic dielectrics and ferroelectrics, semiconductors, and organic and semi-organic molecular crystals. A distinctive feature of molecular crystals is the presence of numerous low-frequency vibrational modes (phonons) associated with weak intermolecular interactions. When a crystal is excited by a femtosecond laser pulse, resonant enhancement of the nonlinear response at the lattice's intrinsic vibration frequencies is possible, allowing efficient conversion of broadband pumping energy into intense narrowband terahertz radiation [5–7].

Within this approach, a promising class of compounds is alkaline metal acid phthalates (MAP, where M = K, Rb, Na, Cs, etc.), long and successfully used in various optics fields, for instance as electro-optic modulators and effective monochromators of soft X-ray radiation [8–14]. Their piezoelectric, acousto-optical, and nonlinear optical properties in the visible range have been studied in detail. However, despite the lengthy research history, these crystals remained virtually unexplored in the terahertz frequency range until recently. Although the possibility of broadband terahertz generation in sodium acid phthalate crystal was briefly demonstrated previously [15], the features related to the resonant phonon response which is key to creating narrowband sources have not yet been identified or studied. Our previous investigations of rubidium acid phthalate (RbAP) [6] and guanylurea hydrogen phosphite (GUHP) crystals [5,7] confirmed the high efficiency of narrowband terahertz generation in molecular crystals. In this work, we present a comprehensive study of sodium acid phthalate (NaAP) molecular crystal. The aim was to investigate the anisotropy of the spectral characteristics of terahertz generation in NaAP crystal — a new efficient medium for compact, tunable narrowband terahertz sources. The obtained results help deepen the understanding of sodium acid phthalate crystals' potential in terahertz photonics and optoelectronics.

Methods and materials

Crystal growth

Sodium acid phthalate crystals were grown in 1.5 L crystallizers by temperature reduction of the solution in the range from 45 to 40 °C. Crystallization solutions were synthesized by dissolving $C_6H_4COOH \cdot COONa$ (OCH) salts in triple-distilled water. Solutions, superheated by 5−7 °C above saturation temperature, were filtered through filters with 10 μm pores to remove mechanical impurities. Growth was conducted without stirring; seeds were crystals obtained by spontaneous nucleation.

Optical and Terahertz Properties Study Methods

To study terahertz transmission spectral properties, a terahertz spectrometer *TeraSmart* (™*MenloSystems*) with antennas from ™*Fraunhofer* IIS acting as receivers and emitters was used. According to the specifications, the spectral range exceeds 6 THz, dynamic range over 100 dB, and frequency resolution less than 1.2 GHz. Due to optical response peculiarities of the antenna semiconductor substrate at around 4 THz, a dip occurs in the terahertz pulse spectrum, limiting the spectral range to 0.2–3.6 THz.

Samples were mounted in a copper holder fixed on the cold finger of a helium closed-cycle cryostat capable of cooling samples to cryogenic temperatures below 10 K. The cryostat core includes an RDK-408D2 cold head (™SHI Cryogenics Group) and a nickel-plated cover with window holes. Sample temperature was monitored by a silicon diode sensor DT-670-CU (™*Lake Shore Cryotronics*) with a temperature range 1.4–500 K and accuracy ±22 mK.

Terahertz emission spectroscopy, operating under principles similar to classical terahertz spectroscopy (THz–TDS) was used to investigate terahertz generation in the samples. The excitation source was a laser system producing a femtosecond regenerative titanium-sapphire amplifier beam *SpitfirePro* (™*Spectra Physics*) with central wavelength 802 nm, pulse duration 120 fs, 1 kHz repetition rate, and pulse energy up to 1.8 mJ. A lens with focal length 280 mm focused the laser beam; the sample was placed 160 mm from the lens to form a spot of diameter ~ 2.6 mm. Excitation polarization was controlled by a Glan–Taylor prism and plate $\lambda/2$; terahertz polarization was controlled via a polyethylene grid terahertz polarizer. Terahertz pulses were detected by a 1 mm thick ZnTe (110) electro-optic crystal in a balanced detection scheme. Terahertz power was measured using a Golay cell (™*Tydex*). Experiments were conducted in a dry-air chamber to avoid absorption effects due to water vapor.

UV, visible, and near-IR transmission spectral characteristics of grown crystals were studied using an ™*Shimadzu* UV-3600 spectrophotometer, capable of registering sample transmission spectra in the wavelength range 185–3300 nm.

Results and discussion

Sodium acid phthalate crystal $C_6H_4(COOH)(COONa) \times 1/2H_2O$ belongs to the polar non-centrosymmetric class *mm2* of the orthorhombic system. This crystal differs from most other acid phthalates by the presence of water molecules in the crystal structure [16,17]. For aligning the crystallophysical coordinate system with the crystallographic one, the symmetry space group *B2ab* (№41), previously established in [16,18,19], was chosen. This group represents a non-standard setting of the space group *Aba2* [19] (transition between the two possible by cyclic permutation of axes) and was selected to avoid confusion when using dielectric and optical properties from previous works. The habit of the grown NaAP crystal is similar to that of other acid phthalate crystals [6] and is shown in Fig. 1, *a*, where the directions of the crystallophysical coordinate axes of the chosen space group are also indicated. The crystal is flattened in the direction [001]. The crystallophysical *X*-axis is taken to be the [100] direction, which is polar, since the overall structure of sodium acid phthalate is similar to NH_4 and K acid phthalates [19,20]. The normal to the perfect cleavage plane (001) is taken as axis *Z* in NaAP crystals.

Optical Transmission Properties of NaAP Crystal

Transmission spectra of the c-cut NaAP crystal were recorded in unpolarized light in the spectral range 250–2000 nm (Fig. 1, *b*). In the near-IR region, pronounced absorption bands are observed with maxima near wavelengths of approximately 1130, 1432, 1660, and 1945 nm. The short-wavelength boundary of the transparency region (fundamental absorption edge) for the NaAP crystal is determined at a wavelength of 298 nm. Based on analysis of the absorption edge using the Tauc method [21], the forbidden gap width was estimated. Assuming a direct allowed interband transition E_g was 4.12 ± 0.03 eV.

Terahertz Transmission Properties of NaAP Crystal

Absorption spectra in the terahertz range were studied for two orthogonal orientations of the terahertz electric field relative to the crystal's crystallo-optical axes, denoted as *X* and *Y* (Fig. 1, *a*).

For the orientation along the selected direction *X* at cryogenic temperature of 10 K, six pronounced peaks corresponding to active phonon modes are identified in the absorption coefficient spectrum over the range 0.2–3.25 THz (Fig. 2, *a*). Due to high absorption levels and the resulting limited dynamic range of the terahertz spectrometer at room temperature, only three low-frequency phonon modes are recorded. To evaluate the temperature dependence of mode parameters including peaks whose intensity exceeded the detection limit (truncated peaks) their profiles were qualitatively approximated by the Breit–Wigner–Fano (BWF) function [6]. This function was chosen due to the observed asymmetry and non-Lorentzian shape of the absorption peaks in the crystal at low temperature. Approximation analysis showed that resonant frequencies of all modes exhibit monotonic shift toward the low-frequency region with increasing temperature. For example, the central frequency of the phonon mode located around ~ 1.6 THz, changes from 1.68 THz at 10 K to 1.57 THz at 293 K.

For the terahertz electric field orientation along the selected direction *Y* at 10 K, active phonon modes also appear in the absorption spectrum, but their number in the frequency range 0.2–3.5 THz is five (Fig. 2, *b*). As for the *X*-direction, the aforementioned approximation procedure was used for qualitative determination of peak central frequencies. Phonon modes for the crystallo-optical axis *Y* also show „red“ shift with increasing temperature. For

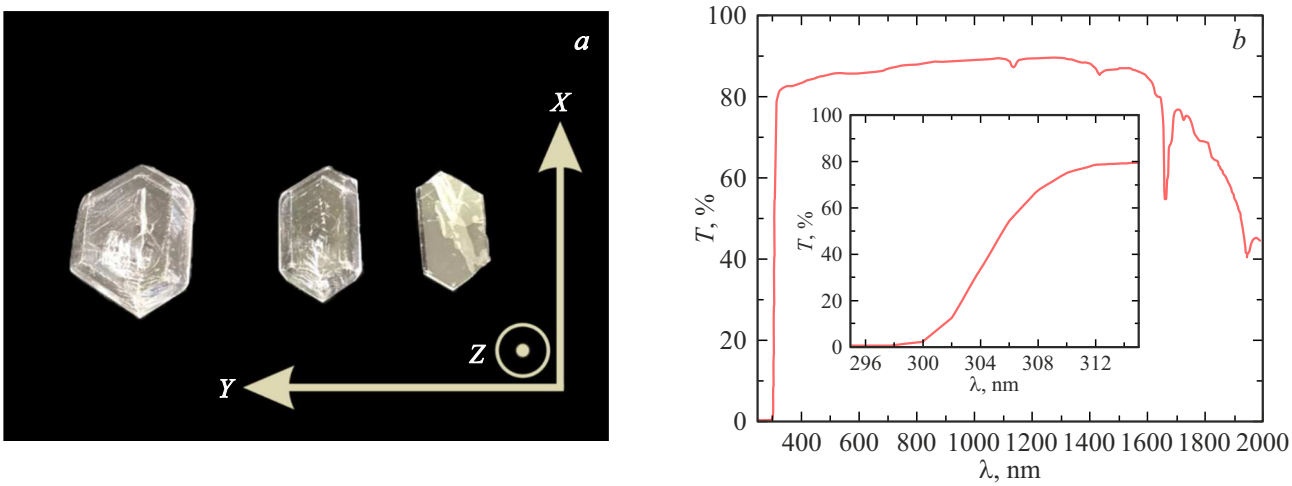

Figure 1. (a) Habit of NaAP crystal and crystallophysical coordinate system XYZ corresponding to the crystallographic abc (a similar habit can be observed for sodium acid phthalate in works [14,20]). (b) Transmission coefficient T of NaAP crystal in UV, visible, and near-IR wavelength ranges in unpolarized light (sample thickness was 375 μm); inset shows transmission spectrum in the range from 295 to 315 nm.

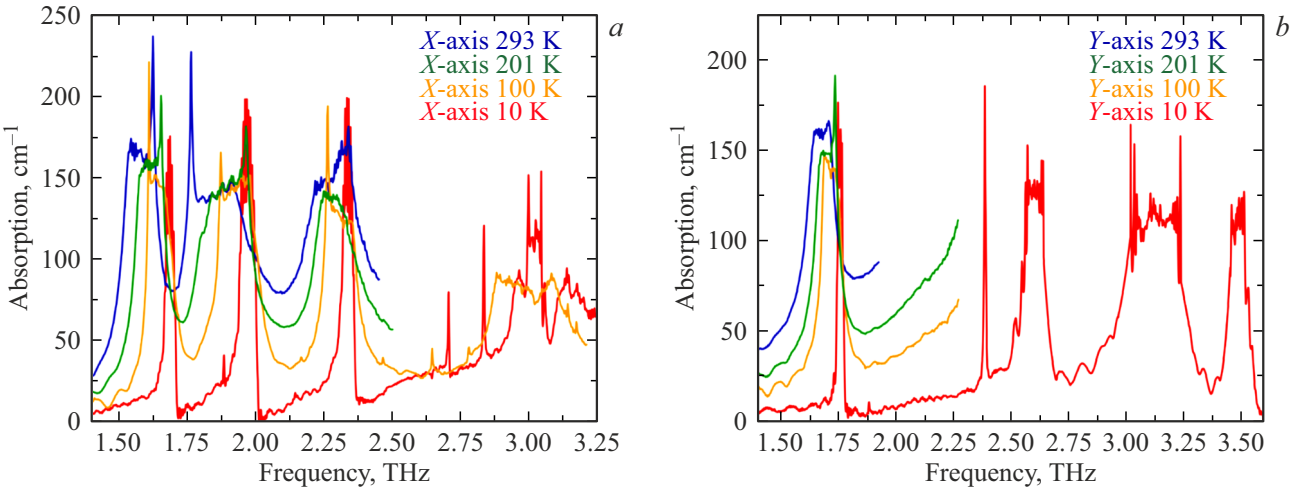

Figure 2. Absorption coefficient spectra by intensity for the two selected directions X (a) and Y (b) of the NaAP crystal with thickness 560 μm in the terahertz frequency range at different temperatures.

instance, the first observed mode in this polarization has its resonant frequency changing from 1.76 THz at 10 K to 1.67 THz at 293 K.

Additionally, Fig. 2 for both crystal orientations shows an increase in the full width at half maximum (FWHM) of the absorption line with rising temperature, which can be explained by thermal atomic motion leading to reduced coherence of vibrations in the sodium acid phthalate crystal lattice.

The NaAP crystal exhibits perfect cleavage along the (001) plane, characterized by the ability to cleave into thin plates effortlessly. This property enabled preparation of thin samples in the thickness range from 40 to 256 μm. Reducing sample thickness shortened the beam path in the crystal and increased the terahertz spectrometer's dynamic range, allowing full resolution of some peaks for the X and Y directions. However, due to experimental technical constraints, measurements were conducted outside the cryostat, i.e., at 293 K.

For the X axis in the spectral range 0.2–2.4 THz three absorption peaks were fully resolved (Fig. 3, a). BWF approximation yielded precise central frequencies (1.57, 1.85, and 2.27 THz) and FWHMs of the identified peaks, from which quality factor parameters $Q = \nu/\Delta\nu$ were calculated. For the first, second, and third peaks, $Q = 20$, 13 and 11, respectively. For the Y axis, approximation characterized only the first peak in the studied spectral range with central frequency 1.67 THz, for which $Q = 28$ (Fig. 3, b). Notably, for the thicker sample where approximation used data not fully resolved within the spectrometer's dynamic range at 293 K similar central frequency values were obtained, confirming the appropriateness of the approximation function.

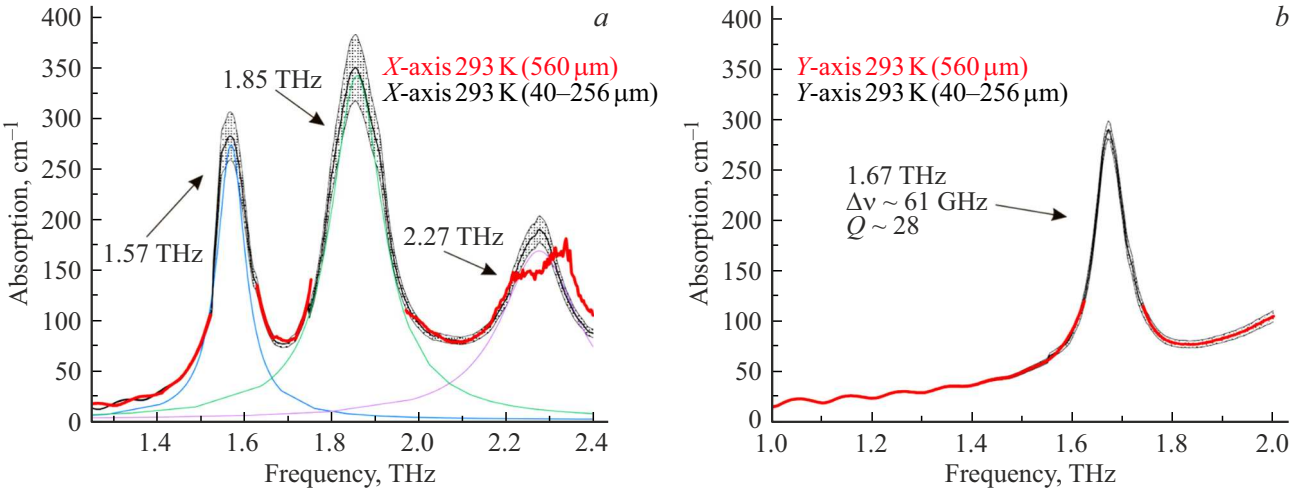

Figure 3. Absorption coefficient spectra by intensity for the two selected directions X (a) and Y (b) of the NaAP crystal for a set of samples in the thickness range 40–256 μm (black line with standard deviation) and a sample of thickness 560 μm (red line) at 293 K.

A slight discrepancy in the high-frequency slope of the third peak for the X-direction (2.27 THz) across different thicknesses is attributable to data loss in the peak center due to dynamic range limits and subsequent errors in Fourier-transforming the detected temporal profile of the scanning terahertz pulse.

Frequency-dependent refractive indices of the NaAP crystal were also obtained. The refractive index behavior for sodium acid phthalate matches that of rubidium acid phthalate [6] features appear near phonon resonances, with monotonic increase at higher frequencies outside these regions. Values for the Y axis exceed those for X in the terahertz range away from resonances (phonon resonance regions were not quantitatively measured due to spectrometer dynamic range limits).

The refractive index temperature dependence is also anisotropic: along the X axis, it increases with temperature, whereas for the Y-orientation up to ~ 1.2 THz preceding the absorption line, changes with temperature are negligible. At 0.5 THz far from phonon resonances, baseline refractive index values for the Y and X-axes are: $n_{\mathrm{Y}}^{\mathrm{THz}} = 2.58$ (10 K), 2.58 (100 K), 2.59 (201 K), 2.59 (293 K), $n_{\mathrm{X}}^{\mathrm{THz}} = 1.95$ (10 K), 1.97 (100 K), 2.00 (201 K), 2.05 (293 K).

Terahertz Generation in NaAP Crystal

Terahertz generation in NaAP crystals was performed using a standard scheme with normal incidence of the exciting femtosecond laser radiation on the sample surface and detection of the generated terahertz pulse in transmission geometry. The excitation source was radiation from a titanium-sapphire regenerative laser amplifier with central wavelength 802 nm and pulse duration 120 fs. Experimental studies of terahertz generation properties covered a wide sample temperature range from 10 to 293 K. Temporal profiles of terahertz pulses generated in NaAP samples were recorded via time-resolved pulsed terahertz spectroscopy based on electro-optic sampling with a delay step corresponding to 50 fs on the time scale. For detailed temporal profile analysis and subsequent spectral characteristics of generated terahertz radiation, the optical pumping pulse energy incident on the sample was fixed at 400 μJ. Fourier transformation of the obtained temporal waveforms enabled investigation of spectral features of the terahertz generation process for various selected crystallooptic directions and sample temperatures.

Fig. 4, a shows characteristic spectra of terahertz radiation generated in NaAP crystal when both the exciting laser polarization and terahertz analyzer were oriented along the selected crystallooptic direction X (hereafter XX configuration). Data correspond to the two extreme temperatures: 10 and 293 K. At cryogenic temperature of 10 K in the studied spectral range from 0.2 to 3 THz, three well-resolved generation lines are distinctly observed. The second, most intense peak stands out, with central frequency 1.99 THz and FWHM of 102 GHz. Upon heating the crystal to room temperature (293 K), amplitudes of all recorded generation lines decrease significantly, by a factor of several times. For example, in the XX-orientation, the first peak shifts to lower frequencies with central frequency reducing to 1.59 THz, its amplitude decreases by 1.5 times, and FWHM increases to 120 GHz. The second peak similarly shifts to lower frequencies reaching 1.92 THz; FWHM grows to 190 GHz, and amplitude drops by 1.5 times like the first peak. Critically, the generation line behavior their central frequencies and relative intensities fully correlates with absorption spectra data for the corresponding X-sample orientation, unequivocally indicating the resonant nature of terahertz generation linked to simultaneous excitation of IR- and Raman-active phonon modes in the crystal [5,6].

Fig. 4, b presents a similar set of experimental data obtained under the same conditions as the previous case, but here the exciting laser radiation was polarized along

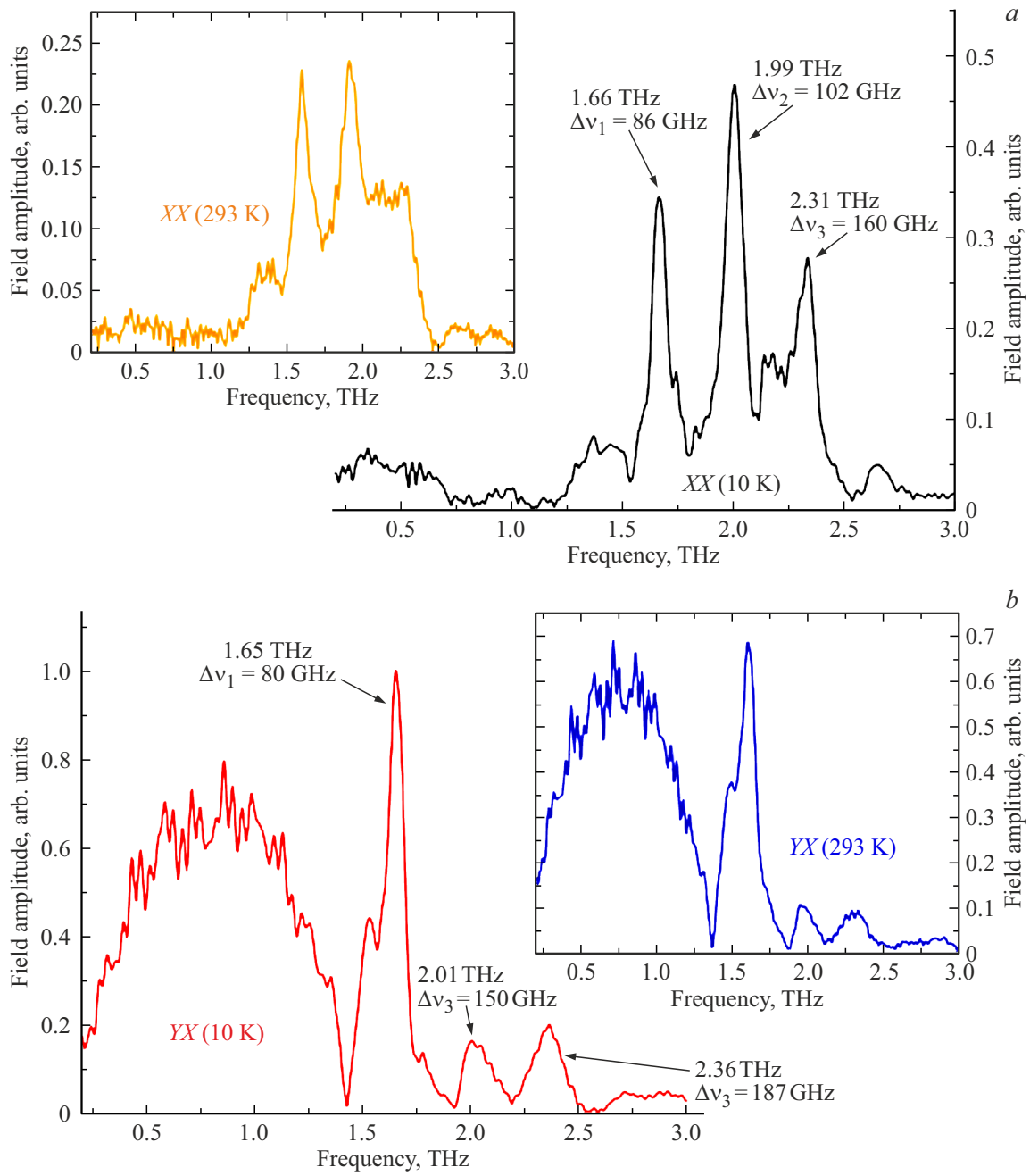

Figure 4. Spectra of terahertz radiation generated in NaAP crystal for the XX (a) and YX (b) cases at 10 and 293 K.

the Y axis, while the terahertz analyzer orientation remained along the X axis (YX configuration). Qualitatively, the generation spectra in this configuration show no fundamental differences from the XX case, but quantitative characteristics undergo substantial changes. In particular, the amplitude of the first, dominant generation peak at the same central frequency of 1.65 THz in the YX configuration increases significantly, by several times, compared to the XX-configuration, accompanied by noticeable narrowing the spectral width decreases to 80 GHz. Notably, the second and third, higher-frequency generation lines in this orientation exhibit reduced amplitudes and slight spectral broadening, with widths increasing compared to the XX-configuration. Upon heating the crystal, the YX-configuration shows less amplitude drop in peaks relative to the XX-case; central frequencies shift to 1.59, 1.97, and 2.2 THz for the 1st, 2nd, and 3rd peaks, respectively, with FWHMs increasing to 120, 200, and 290 GHz. Also noteworthy is the broadband generation component observed in the low-frequency spectral region, approximately from 0.2 to 1.2 THz, which becomes more pronounced in the YX, configuration this is characterized by a fast nonlinear optical response of the crystal's electronic subsystem [5,6]. This redistribution of generation efficiency is explained by differences in the material's dispersive

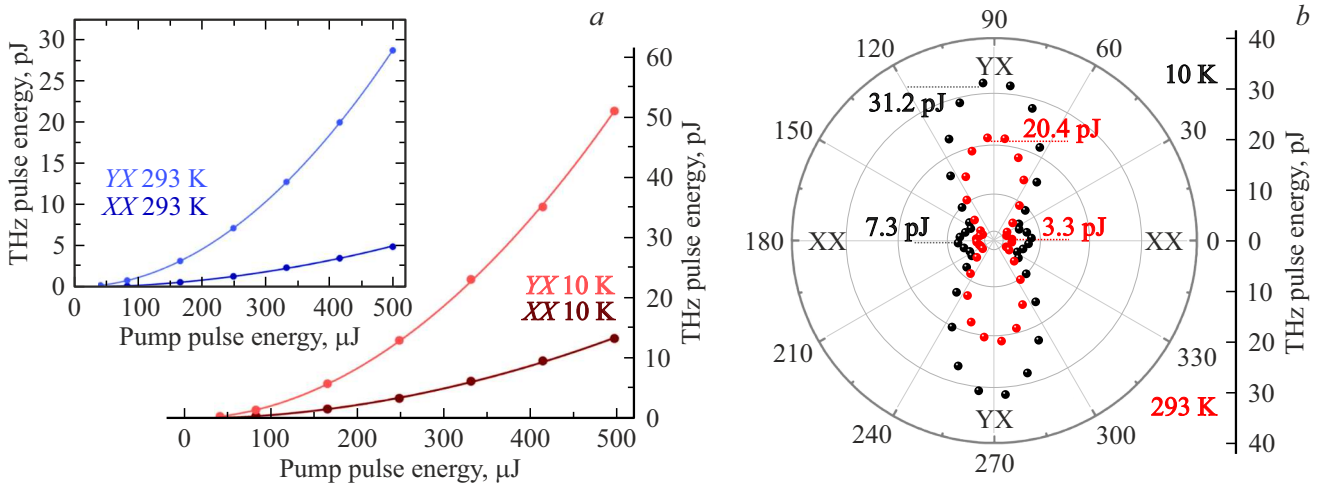

Figure 5. Dependence of generated terahertz radiation energy on the exciting laser radiation energy (*a*) and on the azimuthal angle of laser radiation polarization relative to the *X* axis (*b*) at temperatures of 10 and 293 K.

properties for orthogonal directions and, consequently, varying degrees of phase-matching condition fulfillment. The optical rectification process efficiency requires matching the group refractive index of laser pumping (n_g) and the phase refractive index of the generated terahertz wave (n^{THz}). For NaAP crystal, refractive indices at the pump wavelength of 632.8 nm are $n_x \approx 1.48$, $n_y \approx 1.64$ and $n_z \approx 1.65$ [13] (notably, that work lists the space group as *Aba2*, whereas we adopted the *B2ab* setting, requiring cyclic axis permutation: $n_x \to n_y$, $n_y \to n_z$, $n_z \to n_x$), in the terahertz range, they are — $n_X^{\mathrm{THz}} \approx 1.95$ and $n_Y^{\mathrm{THz}} \approx 2.58$ (10 K). In both configurations (*XX* and *YX*) the *X*-component of the terahertz field is detected. Comparing phase mismatches indicates that for the *YX* configuration, it is smaller than for *XX*. Since phase matching is satisfied much better in the *YX*-configuration, this leads to the observed multiple-fold increase in the dominant generation peak amplitude (Fig. 4). Generation efficiency is also significantly determined by the nonlinear optical susceptibility $\chi^{(2)}$which exhibits resonant behavior in the phonon mode spectral region, varying by selected direction for both terahertz radiation and the pump pulse.

An important additional result is that when the terahertz analyzer is oriented along the *Y* axis, the generation signal, regardless of pumping polarization, was at the noise level. This effect is also explained by the crystal's dispersive properties. For generating *Y*-polarized terahertz radiation ($n_Y^{\mathrm{THz}} \approx 2.58$) the phase mismatch becomes critically large for both pump laser polarizations along *X* and *Y*. Such strong dephasing between the pump pulse and generated wave effectively suppresses the generation process. Additionally, the complete absence of signal may arise from selection rules imposed by the $\chi^{(2)}$tensor, whose components responsible for *Y*-polarized field generation may be negligibly small [6].

Fig. 5, *a* shows results of experimental investigation into the dependence of terahertz pulse energies generated in NaAP single crystal on the energy and polarization of the exciting femtosecond laser radiation for *XY*- and *XX*-installation orientations at 10 and 293 K. A key finding is that at 10 K, the recorded terahertz pulse energy is noticeably higher using the *YX* configuration compared to *XX*. This same trend in generation efficiency persists upon raising the sample temperature to room level (293 K), though absolute generated terahertz pulse energies decrease by several times, attributable in part to increased terahertz frequency absorption and altered phase-matching conditions. Within the measurements conducted here, maximum generated terahertz radiation energy reached 52 pJ at optical pumping energy of 500 μJ. Notably, these experiments did not aim at optimization or maximum conversion efficiency; considering potential further pump energy increase up to the crystal laser damage threshold, substantially higher generation efficiency can be anticipated. The experimentally obtained dependence of terahertz pulse energies on exciting laser pulse energy, as seen in the figure, is well approximated by a quadratic function. Such behavior is characteristic of second-order nonlinear optical response (quadratic nonlinearity) underlying the observed terahertz generation, e.g., via optical rectification [6].

Measurement of generation efficiency dependence on exciting laser radiation polarization orientation relative to crystallooptic axes was conducted at pumping energy 400 μJ (Fig. 5, *b*). In these measurements, the pump laser polarization was rotated by 360°, starting from the orientation corresponding to the previously described *XX* configuration (pump and analyzer polarizations parallel to the crystal's *X* axis) and sequentially passing through all intermediate angles to return to the initial configuration. Importantly, for recording average generated terahertz radiation power in these experiments as in the pumping energy dependence study a Golay cell was used, with laser excitation parameters (wavelength, pulse duration, and energy) kept identical to prior measurements for result com-

parability. Analysis of the obtained angular dependences revealed pronounced anisotropy in terahertz generation efficiency. Specifically, at sample cryogenic temperature of 10 K, the configuration with pumping polarization along the Y axis and terahertz analyzer polarization along X yielded significantly higher generated terahertz radiation energy — up to 31.2 pJ. Meanwhile, for the orthogonal pump orientation along X (XX configuration), the detected terahertz radiation energy was substantially lower, around 7.3 pJ. These observations fully agree with prior data on terahertz pulse energy dependence on pumping energy, where the approximating parabolic dependence for the YX-configuration lay significantly higher than for XX-indicating superior nonlinear conversion efficiency. The overall trend of anisotropic generation and its temperature dependence persists upon raising sample temperature to room level (293 K). Similar to cryogenic conditions, absolute detected terahertz radiation energies decrease (to 20.4 pJ for YX-oriented pump and 3.3 pJ for XX-oriented pump at 293 K). Nevertheless, even at room temperature, the configuration with pump polarization close to the Y axis (at X-analyzer) continues to show substantially higher generated terahertz radiation compared to pumping polarized along X, confirming preservation of pronounced anisotropy in NaAP crystal's nonlinear optical response over a wide temperature range.

Conclusion

This work presents the results of investigating a new nonlinear optical source — the sodium acid phthalate molecular crystal — and demonstrates for the first time its high efficiency for narrowband terahertz radiation generation.

It has been established that the presence of a set of high-quality-factor phonon modes in NaAP crystal, which are simultaneously IR- and Raman-active, allows the realization of resonant optical rectification when excited by ultrashort laser pulses. This enables the generation of terahertz radiation with a minimal spectral linewidth on the order of 80 GHz. Strong anisotropy of the generation process is demonstrated: by choosing the polarization of the laser pump, it is possible not only to increase the overall conversion efficiency several times but also to control the distribution of energy among the generated spectral lines. It is shown that the spectral characteristics of both absorption and generation strongly depend on temperature, opening the possibility for temperature tuning of the central frequency of the emission.

Thus, the demonstrated ability to generate narrowband terahertz radiation and to control its characteristics via pump polarization and temperature makes the NaAP crystal a promising material for creating compact terahertz sources.

Conflict of interest

The authors declare that they have no conflict of interest

Funding

This work was carried out within the framework of the state assignment of the National Research Center „Kurchatov Institute“ for the growth of crystal samples and terahertz spectroscopy studies, and within the framework of the state assignment of Lomonosov Moscow State University for research on the properties of terahertz radiation generation.

References

[1] A. Leitenstorfer, A.S. Moskalenko, T. Kampfrath, J. Kono, E. Castro-Camus, K. Peng, N. Qureshi, D. Turchinovich, K. Tanaka, A.G. Markelz, M. Havenith, C. Hough, H.J. Joyce, W.J. Padilla, B. Zhou, K.-Y. Kim, X.-C. Zhang, P.U. Jepsen, S. Dhillon, M. Vitiello, E. Linfield, A.G. Davies, M.C. Hoffmann, R. Lewis, M. Tonouchi, P. Klarskov, T.S. Seifert, Y.A. Gerasimenko, D. Mihailovic, R. Huber, J.L. Boland, O. Mitrofanov, P. Dean, B.N. Ellison, P.G. Huggard, S.P. Rea, C. Walker, D.T. Leisawitz, J.R. Gao, C. Li, Q. Chen, G. Valušis, V.P. Wallace, E. Pickwell-MacPherson, X. Shang, J. Hesler, N. Ridler, C.C. Renaud, I. Kallfass, T. Nagatsuma, J.A. Zeitler, D. Arnone, M.B. Johnston, J. Cunningham. J. Phys. D: Appl. Phys., **56** (22), 223001 (2023). DOI: 10.1088/1361-6463/acbe4c

[2] S.S. Dhillon, M.S. Vitiello, E.H. Linfield, A.G. Davies, M.C. Hoffmann, J. Booske, C. Paoloni, M. Gensch, P. Weightman, G.P. Williams, E. Castro-Camus, D.R.S. Cumming, F. Simoens, I. Escorcia-Carranza, J. Grant, S. Lucyszyn, M. Kuwata-Gonokami, K. Konishi, M. Koch, C.A. Schmuttenmaer, T.L. Cocker, R. Huber, A.G. Markelz, Z.D. Taylor, V.P. Wallace, J.A. Zeitler, J. Sibik, T.M. Korter, B. Ellison, S. Rea, P. Goldsmith, K.B. Cooper, R. Appleby, D. Pardo, P.G. Huggard, V. Krozer, H. Shams, M. Fice, C. Renaud, A. Seeds, A. Stöhr, M. Naftaly, N. Ridler, R. Clarke, J.E. Cunningham, M.B. Johnston. J. Phys. D. Appl. Phys., **50** (4), 043001 (2017). DOI: 10.1088/1361-6463/50/4/043001

[3] M. Takahashi. Crystals, **4** (2), 74–103 (2014). DOI: 10.3390/cryst4020074

[4] X. Fu, Y. Liu, Q. Chen, Y. Fu, T.J. Cui. Front. Phys., **10**, 869537 (2022). DOI: 10.3389/fphy.2022.869537

[5] A.S. Sinko, N.V. Surovtsev, A.V. Kargovsky, N.A. Nikolaev, V.L. Manomenova, N.N. Kozlova, E.B. Rudneva, A.E. Voloshin, A.P. Shkurinov. IEEE Trans. Terahertz Sci. Technol., **13** (5), 526–538 (2023). DOI: 10.1109/TTHZ.2023.3286662

[6] A.S. Sinko, N.N. Kozlova, V.L. Manomenova, E.B. Rudneva, A.E. Voloshin, N.E. Novikova, Ph.A. Kozhevnikov, M.R. Konnikova, A.P. Shkurinov. J. Surf. Invest.: X-Ray, Synchrotron Neutron Tech., **18** (6), 1516–1529 (2024). DOI: 10.1134/S1027451024701490

[7] A. Sinko, P. Solyankin, A. Kargovsky, V. Manomenova, E. Rudneva, N. Kozlova, N. Sorokina, F. Minakov, S. Kuznetsov, N. Nikolaev, N. Surovtsev, I. Ozheredov, A. Voloshin, A. Shkurinov. Sci. Rep., **11** (1), 23433 (2021). DOI: 10.1038/s41598-021-02862-3

[8] N. Kejalakshmy, K. Srinivasan. J. Phys. D. Appl. Phys., **36** (15), 1778 (2003). DOI: 10.1088/0022-3727/36/15/305

[9] G.S. Belikova, L.M. Belyaev, M.P. Golovej, Yu.V. Pisarevskij, I.M. Sil'vestrova, T.I. Turskaya. Kristallografiya, **19** (3), 566–572 (1974). (in Russian)

[10] L.M. Belyaev, G.S. Belikova, A.B. Gil'varg, I.M. Sil'vestrova. Kristallografiya, **14** (4), 645–651 (1969). (in Russian)
[11] M. Barsukova, G. Belikova, L. Belyaev, V. Boiko, A. Gil'varg, S. Pikuz, A. Faenov, A. Chugunov. Instrum. Exp. Tech., **23** (4), 1028 (1980).
[12] K. Yamashita, M. Watanabe, O. Matsudo, J. Yamazaki, I. Hatsukade, T. Ishigami, S. Takahama, K. Tamura, M. Ohtani. Rev. Sci. Instrum., **63** (1), 1217–1220 (1992). DOI: 10.1063/1.1143087
[13] A. Miniewicz, S. Bartkiewicz. Adv. Mater. Opt. Electron., **2** (4), 157–163 (1993). DOI: 10.1002/amo.860020402
[14] S. Chandran, R. Paulraj, P. Ramasamy, K.K. Maurya. J. Inorg. Organomet. Polym. Mater., **27**, 1383-1390 (2017). DOI: 10.1007/s10904-017-0592-y
[15] S. Yadav, M. Kumari, D. Nayak, G. Moona, R. Sharma, N. Vijayan, M. Jewariya. J. Nonlinear Opt. Phys. Mater., **31** (02), 2230001 (2022). DOI: 10.1142/S0218863522300018
[16] R.A. Smith. Structural Science, **31** (9), 2345–2347 (1975). DOI: 10.1107/S0567740875007546
[17] Yu.A. Sokolov, V.Yu. Galickij, G.S. Belikova, T.M. Ohrimenko. Kristallografiya, **21** (4), 836–837 (1976). (in Russian)
[18] Y. Okaya, R. Pepinsky. Acta Crystallogr., **10** (4), 324–328 (1957). DOI: 10.1107/S0365110X57000936
[19] V.F. Bereznickaya, V.I. Andrianov, V.I. Simonov. Kristallografiya, **21** (5), 922–928 (1976). (in Russian)
[20] H. Schwarz, R. Fiedler, H. Follner. Cryst. Res. Technol., **20** (3), 351–359 (1985). DOI: 10.1002/crat.2170200310
[21] J. Klein, L. Kampermann, B. Mockenhaupt, M. Behrens, J. Strunk, G. Bacher. Adv. Funct. Mater., **33** (47), 2304523 (2023). DOI: 10.1002/adfm.202304523

Translated by J.Savelyeva